Cyclodextrin-covered organic nanotubes derived from self-assembly of dendrons and their supramolecular transformation

Chiyoung Park, Im Hae Lee, Sanghwa Lee, Yumi Song, Mikyo Rhue, and Chulhee Kim*

Department of Polymer Science and Engineering, Hyperstructured Organic Materials Research Center, Inha University, Incheon 402-751, Korea

Edited by Robert Langer, Massachusetts Institute of Technology, Cambridge, MA, and approved December 1, 2005 (received for review June 26, 2005)

The dendritic building blocks with a focal pyrene unit self-organize into vesicles in aqueous phase. The *in situ* inclusion of the focal pyrene units into the cavity of β- or γ-cyclodextrin (CD) induces self-assembled organic nanotubes with an average outer diameter of ≈45 nm and inner diameter of 22 nm. The surface of the nanotube is covered with CD. Therefore, the functional group on the surface of the nanotube is controlled simply by modifying the functionality of CD. The removal of CD from the nanotube with poly(propylene glycol) reversibly generates vesicles. This work provides an efficient methodology not only to create an additional class of CD-covered organic nanotubes but also to exhibit reversible transformation of nanotubes and vesicles triggered by the motifs of dendron self-assembly, CD inclusion, and pseudorotaxane formation.

vesicle | amphiphile

Self-assembly and transformation of biological or synthetic macromolecules in a wide range of scientific fields are crucial subjects for the achievement of well defined nanostructures and the precise control of the function of supramolecules at the molecular level (1–14). A multitude of biological or chemical assemblies including vesicle, tubule, fibril, and viral helical coats perform numerous biochemical operations in nature. In particular, vesicular and tubular assemblies are of much interest because of their unique characteristics as a biomimetic system, carrier for drug or gene, biochemical sensor, electronic or photonic material, nanoreactor, and template for hybrid structure (9–18). Therefore, in these viewpoints, self-assembly of synthetic building blocks by noncovalent interactions is expected to provide a unique methodology for creating supramolecular functional materials (5–15, 17–27).

Self-organization of dendrons (6) into supramolecular assemblies has been demonstrated in a thermotropic fashion (19, 27), in aqueous phase (21–25), in organic media (20, 22, 23, 26), and at solid–liquid interface (26). Recently, we reported that the amide dendrons can self-organize in various conditions to exhibit a multiplicity of architectures and functions (22–26). For the preparation of self-assembling nanomaterials, we designed the amide dendritic building blocks consisting of amide branches for hydrogen bonding, carboxyl functionality at the focal point, and alkyl tails for the stabilization of assembled structures by van der Waals interaction (22). Particularly, it was suggested that the dimeric form of the amide dendron, induced by secondary interactions such as hydrogen bonding and π–π interaction at the focal functional units, is the primary building block in the self-aggregation process in organic media (22, 23, 26). In addition, the amphiphilic nature of these amide dendritic building blocks provides an opportunity for the formation of various self-assembled nanostructures in aqueous phase. For example, we reported that the transition of the self-organized structure from vesicles to rods and spherical micelles was triggered by the increase of the molecular weight of the hydrophilic polyethylene glycol focal moiety (24). Therefore, we reasoned that the nature of the focal functionality of the amide dendrons could determine the supramolecular structure in aqueous phase.

Here we report a supramolecular route to a class of organic nanotubes derived from self-assembly of dendrons and cyclodextrin (CD) inclusion complex so that the outer and inner surface of the nanotube is covered with CD. In addition, a reversible supramolecular transformation of the nanotubes and vesicles is demonstrated by controlling the nature of the focal moiety of the dendritic building block in a noncovalent fashion such as CD inclusion and pseudorotaxane motifs (Fig. 1).

Results and Discussion

The self-assembly characteristics of the amide dendrons with focal pyrene units in Fig. 2 were investigated in aqueous phase. The inclusion of pyrene moiety into CD can make a drastic change in the nature of the focal moiety of the dendron from hydrophobic pyrene to hydrophilic exterior of CD (ref. 28 and references therein). Therefore, we reasoned that CD inclusion would trigger the transformation of supramolecular structures induced by self-assembly of the dendrons with a focal pyrene unit. In addition, removal of CDs from the focal inclusion complex moiety by using a CD-poly(propylene glycol) (PPG) pseudorotaxane motif (29) would provide a unique route to the reversal of the supramolecular structure. In addition, pyrene has unique fluorescence characteristics depending on the environmental condition, which is very useful for monitoring the transformation of the organized structures.

The amide dendrons with a pyrene focal unit in Fig. 2 were prepared by coupling amide dendron 1 with pyrene derivatives through different spacers (see Fig. 7, which is published as supporting information on the PNAS web site). Dendrons **2–5** with a pyrene unit at the focal moiety formed very stable vesicular organizations for several months in aqueous phase without any precipitation. The typical vesicle images through transmission electron microscopy (TEM) and environmental scanning electron microscopy (E-SEM) are shown in Fig. 3. The gel filtration experiment coupled with dynamic light scattering (DLS) confirmed the existence of water entrapped in the interior of the spherical supramolecular assembly (see Fig. 8, which is published as supporting information on the PNAS web site). The average diameter of the vesicles from dendrons **2–5** measured by DLS was 259 nm [polydispersity index (PDI) = 0.125], 253 nm (PDI = 0.145), 238 nm (PDI = 0.209), and 209 nm (PDI = 0.148), respectively.

The organized state of the focal pyrene units in the vesicle was investigated by using fluorescence techniques. All of the aqueous

Conflict of interest statement: No conflicts declared.

This paper was submitted directly (Track II) to the PNAS office.

Abbreviations: CD, cyclodextrin; TEM, transmission electron microscopy; EF-TEM, energy-filtering TEM; E-SEM, environmental scanning electron microscopy; DLS, dynamic light scattering; AFM, atomic force microscopy; PPG, poly(propylene glycol).

*To whom correspondence should be addressed. E-mail: chk@inha.ac.kr.

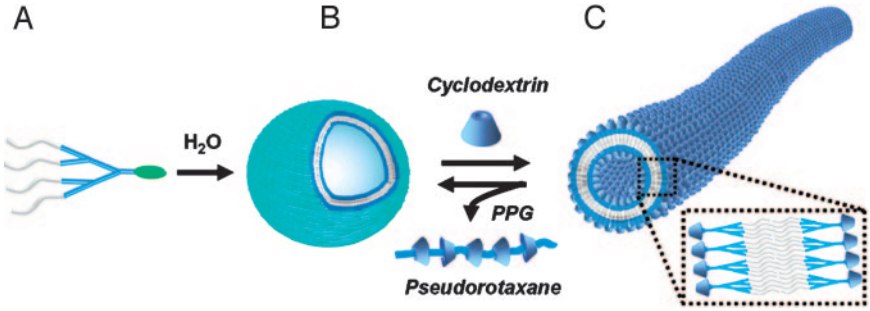

Fig. 1. Schematic route to organic nanotubes and the reversible transformation of supramolecular assemblies of dendrons triggered by the motifs of CD inclusion and pseudorotaxane formation. (*A*) Amphiphilic dendron-pyrene conjugate. (*B*) Vesicular organization of dendron-pyrene conjugates in water. (*C*) The CD-covered nanotubes obtained by the supramolecular transformation after addition of CDs to the vesicular solution. The reverse transformation from nanotube to vesicle can be accomplished by removal of CDs on the surface of the nanotube by using PPG.

vesicular solutions revealed a broad emission of pyrene excimer (E) at ≈420–550 nm with an excitation at 345 nm (Fig. 4*A*), which suggests that the focal pyrene units are preorganized to form excimers. The vesicular solutions of dendron **2** and **3** showed only a broad excimer emission band at 485 and 479 nm, respectively, without emission of monomeric pyrene (M). The vesicular solution of **4** and **5**, which have longer spacer units than those of **2** and **3**, also showed a broad excimer emission band with a maximum at 485 and 478 nm, respectively, with small emission bands of monomeric pyrene at ≈370–410 nm. The I_E/I_{M1} values, the ratio of intensities of the emission maximum of excimer (I_E) and monomeric pyrene (I_{M1}), for **4** and **5** were 4.17 and 2.64, respectively. For the vesicular solutions of **2** and **3**, the I_E/I_{M1} values were much higher, i.e., 30.21 and 25.34, respectively. This result indicates that the excimer formation is more pronounced for the dendrons with shorter spacer, possibly because the mobility of the focal moiety is reduced and thus preassociation of the pyrene moieties is enhanced.

The supramolecular transformation of vesicle into nanotube was induced by introducing the focal pyrene units included into the cavity of CD, which makes the focal moiety very hydrophilic because of the hydroxyl groups of the CD exterior. Indeed, addition of γ-CD to the aqueous vesicular solution of dendron **3** with sonication for 1 min caused disappearance of the excimer band of pyrene (≈420–550 nm), and the emission bands of monomeric pyrene (≈370–410 nm) appeared as shown in Fig. 4*B*. This result shows that the inclusion of the focal pyrene moiety into the cavity of γ-CD interrupts the formation of pyrene excimer. The I_M/I_E value, the fluorescence intensity ratio of pyrene excimer and monomer, increases until the molar ratio of γ-CD/**3** becomes 1, which suggests that the inclusion complex formation between the focal pyrene unit and γ-CD in this system is almost 1:1 (see Fig. 9, which is published as supporting information on the PNAS web site). In the case of β-CD, similar results were observed. However, the addition of α-CD into the vesicular solution did not produce any noticeable changes in either fluorescence or DLS study, which indicates that α-CD does not bind to the pyrenyl group of the dendron so the supramolecular transition was not induced (see Fig. 9).

The dramatic transformation of the supramolecular structures from vesicle to nanotube after the addition of γ-CD or β-CD to the vesicular solution of dendron **3** was confirmed by using TEM, SEM (Figs. 4 and 5), and atomic force microscopy (AFM) (see Fig. 10, which is published as supporting information on the PNAS web site). From the TEM image in Fig. 5 *B* and *C* a clear tubular structure is observed. In addition, the structure of nanotube was visualized by observing the water-soluble staining agent, phsophotungstic acid, entrapped in the inner hollow of the nanotube (Fig. 4*C*) (18). Energy-dispersive x-ray analysis demonstrated the presence of tungsten within the interior hollow of the nanotube (see Fig. 11, which is published as supporting information on the PNAS web site). SEM analysis showed an open end of the tubular structure (Fig. 5*A*). Based on experiments with TEM, AFM, and E-SEM, it is clear that the degree of supramolecular transformation in all cases is well over 90%.

Based on the TEM analysis, the outer and inner diameters of the nanotube were ≈45 and 22 nm, respectively, and the wall thickness was 11.5 nm (Fig. 5 *B* and *C*). Considering the dimension of the fully stretched structure of dendron **3** (53.5 Å, see Table 1, which is published as supporting information on the PNAS web site), the wall thickness of the nanotube must be associated with the unilamellar bilayer of dendron **3** with the focal pyrene moiety included into the cavity of γ-CD. It is suggested that the hydrophilic exterior of the CD–pyrene inclusion complex at the focal moiety is exposed to the aqueous phase,

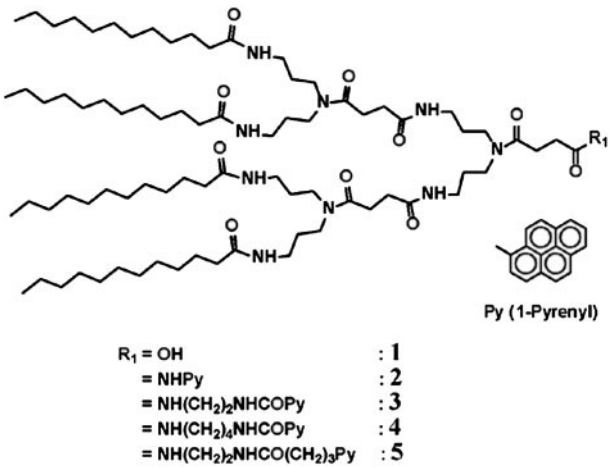

Fig. 2. Structure of the amide dendron-pyrene conjugates.

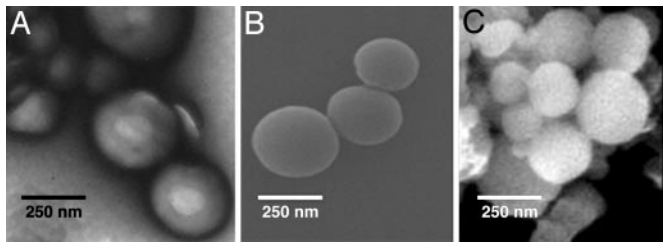

Fig. 3. TEM and E-SEM images. (*A* and *B*) TEM (*A*) and E-SEM (*B*) images of vesicles of **3**. (*C*) E-SEM image of vesicle of **4**.

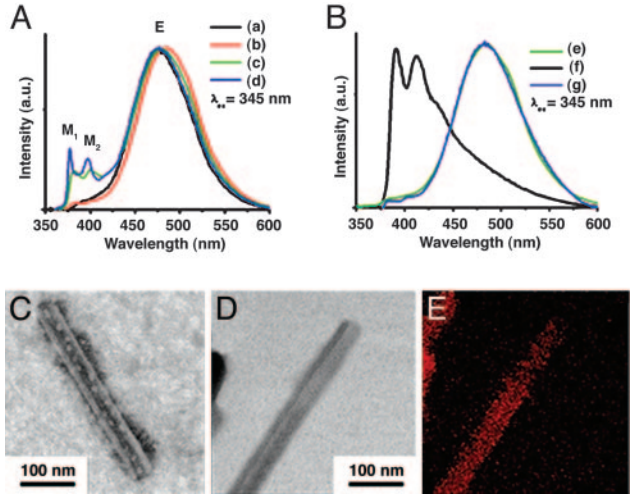

Fig. 4. Fluorescence spectra and TEM analysis. (*A*) Fluorescence emission spectra of vesicular solutions of **2** (*a*), **3** (*b*), **4** (*c*), and **5** (*d*). (*B*) Fluorescence emission spectra of **3** in water (*e*), γ-CD/**3** complex in water (*f*), and γ-CD/**3**/PPG1000 in water (*g*). (*C*) TEM image of the nanotube from γ-CD/**3** complex with phosphotungstic acid encapsulated in the inner hollow of the tube (see *Materials and Methods* and Fig. 11). (*D*) EF-TEM image (zero-loss image) of the nanotube from the per-6-thio-γ-CD/**3** complex in water. (*E*) EF-TEM image for sulfur component with electron energy loss spectroscopy of the nanotube from the per-6-thio-γ-CD/**3** complex in water.

and the hydrophobic alkyl peripheries are located in the middle of the wall membrane of the nanotube. Therefore, the outer and inner surface of the nanotube is covered with CDs. This result also indicates that the surface functionality of the nanotube can conveniently be controlled by the modification of the functionality of CD (30). For example, addition of per-6-thio-γ-CD into the vesicular solution of dendron **3** produced nanotubes with similar dimensions to those obtained with γ-CD. In this case, the surface of the nanotube is covered with thiol functionality introduced at thiolated γ-CD, which was used to include the focal

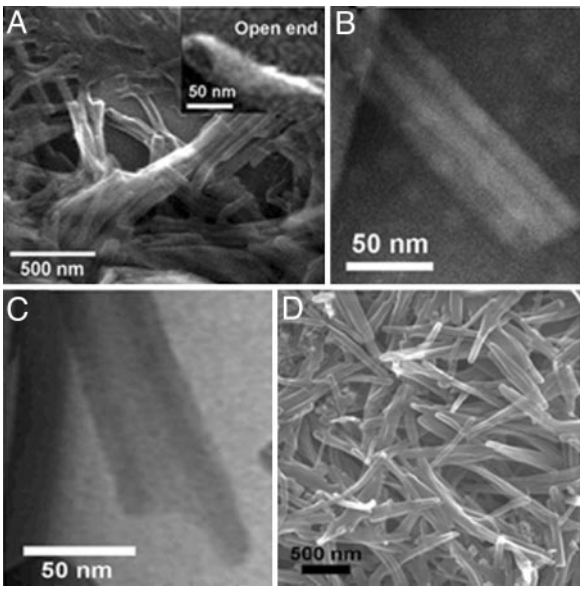

Fig. 5. Images of nanotubes. (*A*) E-SEM image of γ-CD/**3** tube. E-SEM image in upper right shows the open end of nanotube. (*B*) TEM image of γ-CD/**3** tube (uranyl acetate 2%). (*C*) EF-TEM image of β-CD/**3** tube. (*D*) E-SEM image of β-CD/**3** tube.

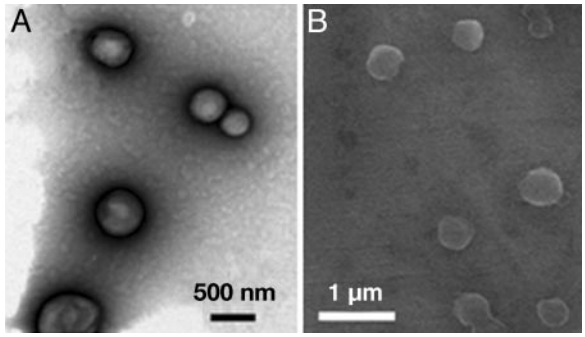

Fig. 6. EF-TEM and E-SEM images. (*A*) EF-TEM image shows the transformation of the supramolecular structures from nanotube to vesicle after the addition of PPG1000 to the tubular solution of γ-CD/**3**. (*B*) E-SEM image also shows spherical vesicles.

pyrene moiety of the dendron. Fig. 4 *D* and *E* shows TEM and an electron energy loss spectroscopic sulfur mapping image of the nanotube prepared from per-6-thio-γ-CD and dendron **3**. This is an example of the organic nanotubes that possess the CD-inclusion complex on the tubular surface (for CD molecular tubes, see ref. 31). The inclusion of hydrophobic pyrene into the cavity of CD is expected to make the focal moiety hydrophilic because of the hydrophilic outer surface of CD, and consequently the volume ratio of the hydrophilic and hydrophobic moieties of the building blocks is changed. The dendron building blocks with the focal CD-pyrene are expected to form bilayer structures, which undergo helical transformation and then form tubular architecture after a similar mechanism of the nanotube formation of lipids (8, 12, 14, 32).

The reversal of the supramolecular structure from nanotube to vesicle was accomplished by removal of focal CD by using a motif of pseudorotaxane formation. Addition of PPG1000 (number average molecular weight = 1,000) to the aqueous solution of the nanotube derived from dendron **3** and γ-CD induces reversal of emission spectra from monomeric to excimeric pyrene (Fig. 4*B*). In addition, the resonances of methyl protons of PPG entrapped in the cavity of γ-CD were observed in ^{1}H NMR spectra (see Fig. 12, which is published as supporting information on the PNAS web site) (29). These results indicate that focal γ-CD is removed from the nanotube and taken up by PPG to form pseudorotaxane. TEM and SEM images exhibit the image of vesicles (Fig. 6).

Conclusions

In summary, we have prepared CD-covered organic nanotubes and demonstrated a reversible supramolecular transformation of nanotubes and vesicles triggered by the combination of the dendron self-assembly, CD inclusion, and pseudorotaxane formation. The amide dendrons self-assemble into a vesicular organization, which can be transformed to the nanotubes with CD-covered surfaces by using a CD-pyrene inclusion motif. In addition, the reversible transformation from the nanotube to vesicle was achieved by using PPG, which removes CD from the nanotube and forms pseudorotaxane. The structure of the nanotube is unique in that the surface is covered with CDs. The functional group on the surface of the nanotubes is controlled just by modifying the functionality of CDs, which are introduced on the surface of the nanotube. The modification of the CD structure and the alkyl periphery should lead to the construction of an additional class of functional nanotubes (33). We expect that our findings will lead to supramolecular materials with a variety of applications.

Materials and Methods

The synthesis and characterization of compounds are described in detail in *Supporting Text*, which is published as supporting information on the PNAS web site.

Typical Sample Preparation. A 30-mg sample was placed into a 100-ml round bottom flask and dissolved with 3–5 ml of tetrahydrofuran (THF). Sixty milliliters of doubly distilled water was added slowly in the flask with gentle stirring. After vigorous stirring for 15 min, THF was evaporated under reduced pressure. The solution with slight blue hue was filtered through a syringe filter (0.45 μm, cellulose acetate membrane). The amide dendrons with pyrene focal moiety, **2**, **3**, **4**, and **5**, formed vesicles in water without sonication. They were stable for several months without formation of any precipitation. To obtain tubular nanostructure, an equimolar amount of CD to dendron was added to a vesicular solution and sonicated for 1 min. Removal of CD from nanotube can be achieved by adding PPG1000 ([CD]/[PPG] = 10:1) into a tubular solution. CD-PPG pseudorotaxane became precipitated in water and was removed from vesicular solution by filtration.

Gel Filtration. A solution of resorufin sodium salt in water (0.14 mM, 10 ml) was added dropwise to a tetrahydrofuron (THF) solution (3 ml) of **3** and **4** (1 mg). THF was completely removed from the sample under reduced pressure at 30°C. The sample solution (500 μl) was then passed through a Sephadex G-100 column (2 × 20 cm) with water as an eluent (34). Forty fractions (2 ml) were collected, and all of the fractions were subjected to DLS and fluorescence measurement. The vesicular structure was further evidenced by investigating the release profile of the entrapped dye molecules before and after addition of Triton X-100. After addition of Triton X-100, which dissolves vesicular membranes, a prompt release of the water-soluble dye molecules from the interior of the vesicle was observed (see Fig. 8). The release profiles were calculated by using the following formula,

$$\text{Release percentage } (\%) = (I_t - I_0)/(I_\infty - I_0) \times 100,$$

where I_0 is initial fluorescence intensity, I_t is fluorescence intensity at time t, and I_∞ is fluorescence intensity after the addition of Triton X-100.

DLS. DLS measurements were performed by using a Brookhaven Instruments (Holtsville, NY) BI-200SM goniometer and BI-9000AT digital autocorrelator. All of the measurements were carried out at room temperature. The sample solutions were purified by passing through a Millipore 0.45-μm filter. The scattered light of a vertically polarized He-Ne laser (632.8 nm) was measured at an angle of 90° and collected on an autocorrelator. The hydrodynamic diameters (d) of vesicles were calculated by using the Stokes-Einstein equation $d = k_BT/3\pi\eta D$, where k_B is the Boltzmann constant, T is the absolute temperature, η is the solvent viscosity, and D is the diffusion coefficient. The polydispersity factor of vesicles, represented as μ_2/Γ^2, where μ_2 is the second cumulant of the decay function and Γ is the average characteristic line width, was calculated from the cumulant method (35, 36). CONTIN algorithms were used in the Laplace inversion of the autocorrelation function to obtain the size distribution (37).

Fluorescence Measurements. All of the fluorescence measurements were performed with a Shimadzu RF-5301PC spectrofluorophotometer. For the measurement of emission spectra, emission and excitation slit widths were set at 1.5 nm with λ_{ex} = 345 nm.

TEM. Energy-filtering TEM (EF-TEM) experiments were performed with a Leo 912 Omega transmission electron microscope (Zeiss), operated at an acceleration voltage of 120 kV. Normal TEM image was obtained by using a Philips (Eindhoven, the Netherlands) CM 200 transmission electron microscope, operated at an acceleration voltage of 80 kV. Unstained specimens for electron microscopy were prepared by placing a drop of sample solution on a 200-mesh, carbon-coated copper grid or micro holey grid. About 3 min after deposition, the drops were then blotted off with filter paper. Staining was performed by using a droplet of a 2 weight percentage uranyl acetate (or phosphotungstic acid) solution. The samples were air-dried before measurement. Zero-loss bright-field images were obtained by electron spectroscopic imaging by using an EF-TEM microscope (Leo 912 Omega, Zeiss) operated at 120 kV. Electron energy-loss spectroscopy was also carried out with a Zeiss LEO 912 Omega, using an accelerating voltage of 120 kV on carbon grids. Elemental maps were obtained by subtracting the background intensities under core-loss edges.

Encapsulation of Water-Soluble Staining Agent into the Hollow of Nanotubes. To confirm the tubular structure, we carried out encapsulation of water-soluble staining agent inside the nanotubes. For a typical procedure, a drop of tubular solution was placed onto a carbon-coated copper grid, which was then frozen in liquid nitrogen for 3 min. The sample was freeze-dried to remove the remaining water completely. Then, we deposited a drop of phosphotungstic acid solution (2% in water) on the sample of the grid. About 5 min after deposition, excess solution was removed and the grid was air-dried. Energy-dispersive x-ray analysis analysis was performed with an EDAX (Mahwah, NJ) detector (see Fig. 11).

E-SEM. E-SEM was carried out on an FEI XL-30 field emission gun E-SEM instrument (Philips) (accelerating voltage: ≈10–15 kV; pressure range: ≈08–0.9 Torr). The E-SEM samples were prepared by transferring a drop of sample solution onto a 200-mesh carbon-coated copper grid or a silicon wafer. About 5–10 min after deposition, excess water was removed by touching the edge of the substrate with filter paper.

AFM. Samples for the AFM study were prepared by transferring a drop of sample solution onto a silicon wafer followed by air drying. AFM images were recorded under ambient condition by using a Park Scientific (Sunnyvale, CA) autoprobe CP with a cantilever of ultra lever 06D, operated in noncontact mode.

We thank Prof. Taihyun Chang at the Pohang University of Science and Technology (Pohang, Korea) and Dr. Sang Cheon Lee at the Korea Institute of Ceramic Engineering and Technology (Seoul, Korea) for invaluable discussion. C.K. thanks the Hyperstructured Organic Materials Research Center (Seoul, Korea) for support. This work was supported by Korea Research Foundation Grant 2004-041-D00209.

1. Klug, A. (1983) *Angew. Chem. Int. Ed. Engl.* **22,** 565–582.
2. Lehn, J.-M. (1997) *Supramolecular Chemistry: Concepts and Perspectives* (Wiley, New York).
3. Whitesides, G. M., Mathias, J. P. & Seto, C. T. (1991) *Science* **254,** 1312–1319.
4. Zhang, S. (2003) *Nat. Biotechnol.* **21,** 1171–1178.
5. Whitesides, G. M. & Grzybowski, B. (2002) *Science* **295,** 2418–2421.
6. Fréchet, J. M. J. (2002) *Proc. Natl. Acad. Sci. USA* **99,** 4782–4787.
7. Ishii, D., Kinbara, K., Ishida, Y., Ishii, N., Okochi, M., Yohda, M. & Aida, T. (2003) *Nature* **423,** 628–632.
8. Bong, D. T., Clark, T. D., Granja, J. R. & Ghadiri, M. R. (2001) *Angew Chem. Int. Ed. Engl.* **40,** 988–1011.
9. Vauthey, S., Santoso, S., Gong, H., Watson, N. & Zhang, S. (2002) *Proc. Natl. Acad. Sci. USA* **99,** 5355–5360.
10. Okada, S., Peng, S., Spevak, W. & Charych, D. (1998) *Acc. Chem. Res.* **31,** 229–239.

11. Bellomo, E. G., Wyrsta, M. D., Pakstis, L., Pochan, D. J. & Deming, T. J. (2004) *Nat. Mater.* **3,** 244–248.
12. Hill, J. P., Jin, W., Kosaka, A., Fukushima, T., Ichihara, H., Shimomura, T., Ito, K., Hashizume, T., Ishii, N. & Aida, T. (2004) *Science* **304,** 1481–1483.
13. Fernandez-Lopez, S., Kim, H.-S., Choi, E. C., Delgado, M., Granja, J. R., Khasanov, A., Kraehenbuehl, K., Long, G., Weinberger, D. A., Wilcoxen, K. M. & Ghadiri, M. R. (2001) *Nature* **412,** 452–455.
14. Shimizu, T., Masuda, M. & Minamikawa, H. (2005) *Chem. Rev.* **105,** 1401–1444.
15. Guo, X. & Szoka, F. C., Jr. (2003) *Acc. Chem. Res.* **36,** 335–341.
16. Martin, C. R. & Kohli, P. (2003) *Nat. Rev. Drug Discovery* **2,** 29–37.
17. Hartgerink, J. D., Beniash, E. & Stupp, S. I. (2002) *Proc. Natl. Acad. Sci. USA* **99,** 5133–5138.
18. Reches, M. & Gazit, E. (2003) *Science* **300,** 625–627.
19. Percec, V., Glodde, M., Bera, T. K., Miura, Y., Shiyanovskaya, I., Singer, K. D., Balagurusamy, V. S. K., Heiney, P. A., Schnell, I., Rapp, A., *et al.* (2002) *Nature* **417,** 384–387.
20. Jang, W.–D., Jiang, D. L. & Aida, T. (2000) *J. Am. Chem. Soc.* **122,** 3232–3233.
21. Newkome, G. R., Moorfield, C. N., Baker, G. R., Behera, R. K., Escamillia, G. H. & Saunders, M. J. (1992) *Angew. Chem. Int. Ed. Engl.* **31,** 917–919.
22. Kim, C., Kim, K. T., Chang, Y., Song, H. H. & Jeon, H.–J. (2001) *J. Am. Chem. Soc.* **123,** 5586–5587.
23. Kim, C., Lee, S. J., Lee, I. H., Kim, K. T., Song, H. H. & Jeon, H.-J. (2003) *Chem. Mater.* **15,** 3638–3642.
24. Kim, K. T., Lee, I. H., Park, C., Song, Y. & Kim, C. (2004) *Macromol. Res.* **12,** 528–533.
25. Chang, Y., Park, C., Kim, K. T. & Kim, C. (2005) *Langmuir* **21,** 4334–4339.
26. Ko, H. S., Park, C., Lee, S., Song, H. H. & Kim, C. (2004) *Chem. Mater.* **16,** 3872–3876.
27. Percec, V., Dulcey, A. E., Balagurusamy, V. S. K., Miura, Y., Smidrkal, J., Peterca, M., Nummelin, S., Edlund, U., Hudson, S. D., Heiney, P. A., *et al.* (2004) *Nature* **430,** 764–768.
28. Dyck, A. S. M., Kisiel, U. & Bohne, C. (2003) *J. Phys. Chem. B* **107,** 11652–11659.
29. Harada, A., Okada, M., Li, J. & Kamachi, M. (1995) *Macromolecules* **28,** 8406–8411.
30. Khan, A. R., Forgo, P., Stine, K. J. & D'Souza, V. T. (1998) *Chem. Rev.* **98,** 1977–1996.
31. Harada, A., Li, J. & Kamachi, M. (1993) *Nature* **364,** 516–518.
32. Schnur, J. M. (1993) *Science* **262,** 1669–1676.
33. Atwood, J. L., Davies, J. E. D., MacNicol, D. D. & Vogtle, F., eds. (1996) *Comprehensive Supramolecular Chemistry: Cyclodextrins* (Pergamon, Oxford), Vol. 3.
34. Ravoo, B. J. & Darcy, R. (2000) *Angew. Chem. Int. Ed.* **39,** 4324–4326.
35. Harada, A. & Kataoka, K. (1995) *Macromolecules* **28,** 5294–5299.
36. Harada, A. & Kataoka, K. (1998) *Macromolecules* **31,** 288–294.
37. Wilhelm, M., Zhao, C., Wang, Y., Xu, R., Winnik, M. A., Mura, J., Riess, G. & Croucher, M. D. (1991) *Macromolecules* **24,** 1033–1040.